EFFECT OF PROCESS THERMAL HISTORY ON THE MICROSTRUCTURE OF COPPER PILLAR SnAg SOLDER JOINTS

Mohammed Genanu[1], Jim Wilcox[2], Eric Cotts[1], Jae Joon Choi[3], Ki Seok Kim[3]
[1]Physics and Materials Science, Binghamton University, Binghamton, NY, USA
[2]Universal Instruments Corporation, Conklin, NY USA
[3]CrucialTec, Seongnam, South Korea
mgenanu1@binghamton.edu

ABSTRACT
Two extremes of reflow time scale for copper pillar flip chip solder joints were explored in this study. Sn-2.5Ag solder capped pillars were joined to laminate substrates using either conventional forced convection reflow or the controlled impingement of a defocused infrared laser. The laser reflow joining process was accomplished with an order of magnitude reduction in time above liquidus and a similar increase in solidification cooling rate. The brief reflow time and rapid cooling of a laser impingement reflow necessarily affects all time and temperature dependent phenomena characteristic of reflowed molten solder. These include second phase precipitate dissolution, base metal (copper) dissolution, and the extent of surface wetting. This study examines the reflow dependent microstructural aspects of flip chip Sn-Ag joints on samples of two different size scales, the first with copper pillars of 70µm diameter on 120µm pitch and the second with 23µm diameter pillars on a 40µm pitch. The length scale of Pb-free solder joints is known to affect the Sn grain solidification structure; Sn grain morphology will be noted across both reflow time and joint length scales. Sn grain morphology was further found to be dependent on the extent of surface wetting when such wetting circumvented the copper diffusion barrier layer. Microstructural analysis also will include a comparison of intermetallic structures formed; including the size and number density of second phase Ag_3Sn precipitates in the joint and the morphology and thickness of the interfacial intermetallics formed on the pillar and substrate surfaces.

Key words: Cu pillars, Laser Reflow, Mass Reflow, LeadFree Solders, Microstructure, Cooling Rate.

INTRODUCTION
Changes in the thermal processing history such as soldering temperature, reflow time, and cooling rate affect the microstructure of Pb-free solder joints [1-21]. Cooling rate is one of the most significant variables affecting the microstructure of solder joints. The number and size of Ag_3Sn precipitates in near eutectic Sn-Ag solder joints are directly affected by the cooling rate from the melt during reflow. Understanding the relation between cooling rate and microstructure, and other reflow parameters and microstructure, is important [8-20].

Previous studies examined the effect of cooling rate during reflow on the microstructure of near eutectic SnAgCu solder joints. These joints display a Sn-rich, dendritic matrix, with interdendritic regions populated with Ag_3Sn and Cu_6Sn_5 precipitates. Ochoa et al. [21] observed that for relatively low cooling rates, Ag_3Sn precipitates formed (~0.5°C/s) with a rod-like or a needle-like geometry (diameters less than 20µm). When higher cooling rates were applied (~24°C/s), spherical Ag_3Sn precipitates with diameters less than 3.7µm were observed, as observed in other studies which used conventional solder reflow methods (~2°C/s) [22-27]. Lee et al. [28] used a water quenching method (60°C/s) and also reported micron sized, spherical Ag_3Sn precipitates. Yang et al. [29] found that the reflow time (1200 to 120,000s) did not affect the Ag_3Sn precipitate morphology, although the thickness of the Cu_6Sn_5 intermetallic compound (IMC) at the soldered interface significantly increased. Through use of a laser reflow process, the present study examined the effects of a cooling rate of 100°C/s on both Ag_3Sn precipitate morphology and number density. Results were compared to those from a standard convection reflow process (1.3°C/s), performed on similar Cu pillar samples.

EXPERIMENTAL PROCEDURES
Two classes of semiconductor products were evaluated: large, high I/O chip (as might be characteristic of a processor or ASIC chip in server class products) and a smaller, thinned chip (as might be found in a consumer mobile product). This permitted the comparison of solder joints with substantially different solder volumes.

Substrates and Chips
The server application and mobile application chips were both joined to laminate substrates through soldered copper pillar interconnects. The laminate substrates and semiconductor chips for both cases were supplied by Hana Micron. The server substrate was a 55mm × 55mm laminate with single buildup layers on an 800µm core (individual layer thicknesses are listed in Table 1). The total substrate thickness was 972µm. Chip join pads were finished with ENEPIG and a coined SAC305 pre-solder layer. The server chip was 760µm thick silicon with plated copper pillar interconnect structures. Copper pillars were

capped with Sn2.5%Ag solder. The substrate pad solder volume (SAC305) was nearly equivalent to the solder volume on the bump (Sn2.5%Ag). The plated solder deposits on Cu pillars were reflowed in a convection oven after the electroplating process to reshape the bumps before silicon dicing. Chip attributes are listed in Table 2.

Table 1. Substrate thickness specifications

Description	Thickness (µm)	
	Server	Mobile
Solder mask	21 ±7.5	15 ±5
Copper layer 1	15 ±5	10
Dielectric	30 ±6	30
Copper layer 2	20 ±10	10
Substrate Core	800 ±60	200
Copper layer 3	20 ±10	10
Dielectric	30 ±6	30
Copper layer 4	15 ±5	10
Solder mask	21 ±7.5	15 ±5
Total laminate substrate	972 ±90	370 ±30

The mobile application substrates were 12mm × 12mm laminates. The layup was similar to the server laminate, but with thinner copper layers on a 200µm core. The different thicknesses are shown in the Table 1, the PCB total thickness was 370µm, with a Cu surface finish. The mobile chip was Si wafers with Cu pillar structures, with Sn2.5%Ag solder. The chips were not reflowed in the oven after the electroplating process, so the bumps did not maintain a round shape. The chip thickness is 180µm (see the parameters in Table 2).

Table 2. Chip (Die) interconnect attributes

Parameter	Value	
	Server	Mobile
Die size	20 mm × 20 mm	6 mm × 6 mm
Die thickness	780 µm	180 µm
Bump pitch	120 µm	40 µm
Bump diameter	70 µm	23 µm
Pillar / solder cap height	60 µm [33µm Cu + 2µm Ni + 25µm (SnAg)]	20 µm [10µm Cu +2µm Ni + 8µm (SnAg)]
Surface finish	Electrolytic Ni	Electrolytic Ni
Bump count	17,317	4,676

Chip Join Soldering (server)

Chip join assemblies for this study were fabricated at CrucialTec using both an infrared laser reflow (LR) method, and a conventional, forced convection reflow method. Laser reflow chip joining was accomplished through laser impingement on individual chips, while the convection process reflowed many chips '*en masse*', a process referred to herein as 'mass' reflow (MR). These two processes were applied to the chip assemblies of the previously described server application packages and mobile application packages. For each substrate, the substrate was metallized with a mating pad array and continuity test nets. Cu pillar bumps on the chips were dipped in flux prior to placement on the laminate substrate for reflow.

An example MR temperature profile for the server chip join process is shown in Figure 1. This relatively slow process, minimized thermal gradients within the package assembly throughout the reflow process. The profile shown used a 117 second preheat time (Soak time) between temperatures of 130°C to 220°C. The time above liquidus (TAL) was 53s (reflow time from 220°C to 254°C). The total process time of preheating and reflow was 170s, with additional temperature ramp down time (Cooling time); the cooling rate was 1.3°C /s.

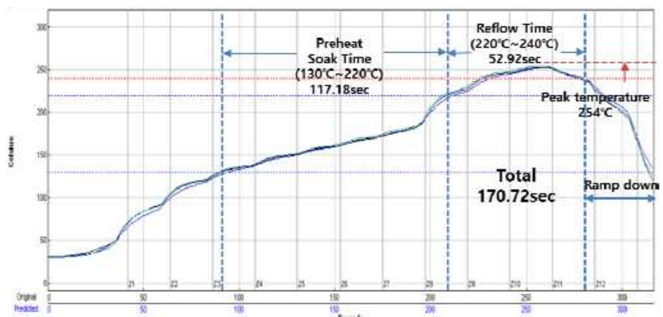

Figure 1. Temperature profile of MR for server package.

In the laser reflow (LR) process the bottom of laminate substrate was heated to 65°C using a preheating stage. An infrared laser beam (λ=980nm) provided a directed heating source enveloping the top of the silicon chip. The beam was shaped to restrict the incident beam to a fixed rectangular area. For the server chip application, the laser power was 350W distributed over a 25mm x 25mm area (Figure 2). The processing parameters used to build the package interconnect are listed in Table 3. The temperature of the top surface of the silicon server chip was measured using an IR camera, assuming an emissivity of 0.7. A calibration of this temperature measurement was performed in one case with thermocouples placed between a Si chip and the PCB such that the thermocouples were in contact with solder. One thermocouple was placed at the outer corner of the chip, and the other at the center (Figure 3). Values of emissivity determined in this fashion were found to be 0.7 [30].

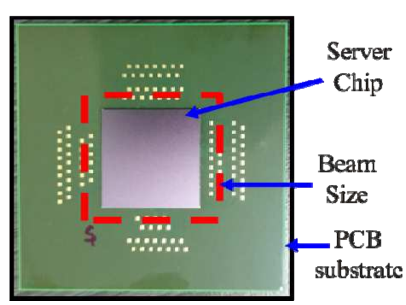

Figure 2. Server chip assembly as presented to laser process. Fluxed chip is exposed to a slightly larger laser beam area to produce uniform heating [30].

Table 3. Laser reflow process parameters

Parameter	Value	
	Server	**Mobile**
Flux Dip Depth	40 µm (WF-6317, Senju)	15 µm (WF-6317, Senju)
Placement Load	10 N	20 N
Temperature Measurement	IR camera	IR camera
	Thermocouple	Thermocouple
Stage Preheating/ Device Temperature	70°C / 65°C	70°C / 65°C
Laser Power Beam Size	~350W 25×25 mm^2	~120W 12×12 mm^2

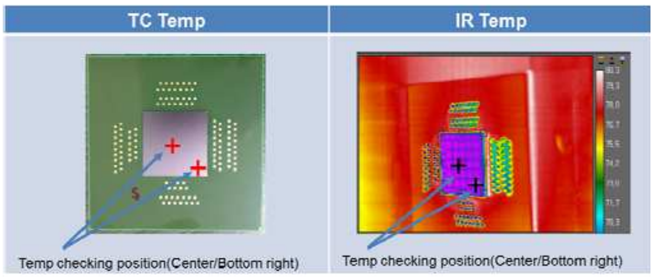

Figure 3. Left: Thermocouples positions between the chip and the substrate. Right: IR temperature measurement locations [30].

The LR process consisted of three steps pre-heating, ramp-up and dwell zones (Figure 4 and Table 4 showing the processing steps). The pre-heating included 1s with laser power at 180W, followed by 2s dwell with power at 350W, followed by a 2s dwell with 235W laser power. The peak solder joint temperature during this reflow process was approximately 293°C, while the time above liquidus was 1s. The cooling rate was greater than 100°C /s.

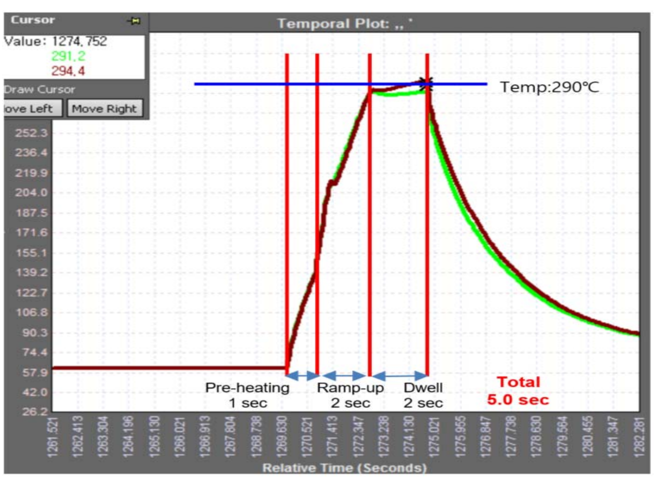

Figure 4. Temperature profile of LR for server chips.

Table 4. The LR profile steps for server and mobile package

Package type	Pre-heating		Ramp-up		Dwell	
	Power (W)	Time (s)	Power (W)	Time (s)	Power (W)	Time (s)
Server package	180	1	350	2	235	2
Mobile package	No Pre-heating		120	0.4	0.74	0.8

Chip Join Soldering (mobile)

Short laser beam irradiation times, with higher light intensities, were used with the mobile chip because it had smaller pitch and bump. For mobile chip LR, a single-step ramp-up was used and 1.2s total process time, with 0.4s ramp-up time and 0.8s dwell time (soak time) was implemented. For server chip LR, a 5s total process time consisting of 1s pre-heating, 2s main ramp-up time and 2s dwell time (soak time) Figure 5 shows the temperate profile and Table 4 shows the processing steps.

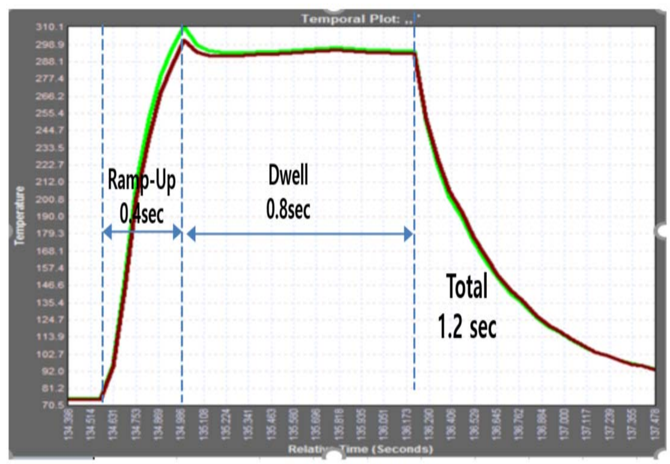

Figure 5. The temperature profile in LR for mobile chips.

The MR took more than two orders of magnitude longer than the LR for the mobile chip package. The peak solder joint temperature was measured on a setup board to be approximately 250°C, while the time above liquidus was 186s and the cooling rate was 0.8°C /s (Figure 6).

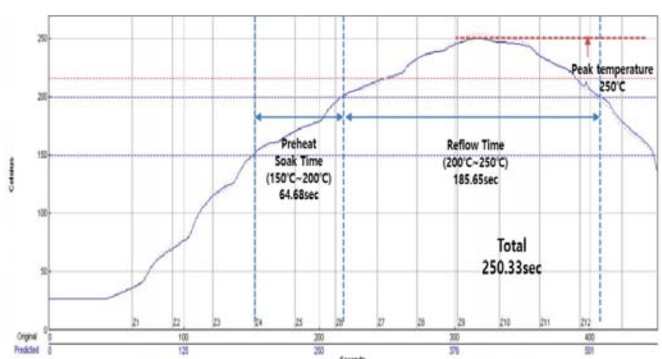

Figure 6. Temperature profile of MR for mobile chips.

Microstructure Characterization

Solder samples before and after chip join were mounted in epoxy for metallographic preparation. All the samples were ground with a sequence of abrasive papers, and polished with diamond suspensions followed by a 0.02 micron colloidal silica suspension. Care was taken at each polishing step to remove all the damage from the previous polishing step. With the final polishing step, the goal was to have no polishing damage left in the Sn from specimen preparation (neither scratches nor surface deformation). The prepared specimens were imaged using optical metallography in both Bright Field (BF) and polarized light with the polarizers nearly crossed (cross-polarizer (XP) imaging). The XP imaging contrast in Sn arises from the birefringent properties of Sn, leading to different colors for different crystal orientations of Sn under XP imaging. XP imaging thus provided a quick and qualitative view of the Sn grain structure for each.

Selected specimens were imaged using scanning electron microscopy (SEM). Backscatter electron (BSE) imaging was used for all quantitative metallography [5]. In BSE composition mode images, contrast is proportional to the average atomic number of the material. Digital image analysis was used to do quantitative measurements on particle distributions. A minimum number of adjacent pixels must meet the contrast threshold to resolve a particle above the signal noise. The fraction of the particulate population visible to the analysis depends on the SEM instrument magnification producing the BSE image. Particle analyses have been done using 4000×, 10,000× and 20,000× instrument magnifications. Only data from the 20,000× measurements will be reported in this paper. At this magnification, particles below 30nm in diameter will not be visible to the image analysis. The magnifications noted in this document's figures refer only to the original instrument magnification. Image sizes as shown have been adjusted for publication [7].

RESULTS AND DISCUSSION

The Sn grain morphologies and the Ag_3Sn precipitate morphologies were examined for two different diameter Cu pillar solder joints (23 and 70 µm), and for two different reflow techniques, MR and LR. Correlations between Ag_3Sn precipitate morphology and reflow technique were examined.

Server Solder Joints (70µm diameter) Ni/Sn2.5Ag/Ni

Laser Reflow

Optical images with crossed polarizers, and SEM images, in Figure 7 show the microstructures of as-reflowed laser reflow process Cu pillar solder joints of the server package. The joint had a Ni surface finish on both the chip side and the substrate (Ni/Sn2.5Ag/Ni) with some Cu incorporated in the solder from the substrate SAC305 pre-solder layer. The Sn grain morphologies, as elucidated by optical microscopy with crossed polarizers, are displayed in the left hand side of Figure 7. It was found that Sn grain morphologies could be characterized as single grained (e.g. Fig. 7(a)), multi-grained (Fig. 7(c)), or interlaced (Fig. 7(e)), as previously observed in other SAC solder joints [15]. The Ag_3Sn precipitate morphologies were examined for LR server solder joints using SEM, as displayed in Figures 7–10.

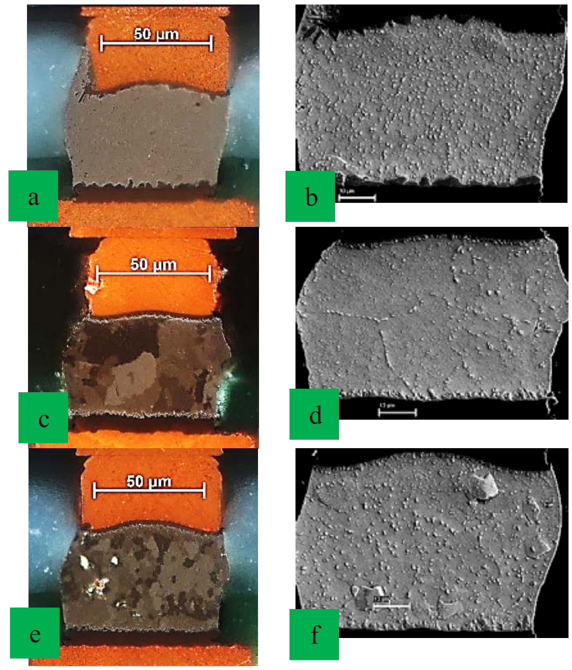

Figure 7. Cu pillar joints (server package 70µm diameter) formed by LR. Left side: cross-polarizer images showing the Sn grain morphology; Right side: corresponding SEM images of the same sample; (a) and (b) single grain, (c) and (d) multi-grain, (e) and (f) interlaced Sn grains.

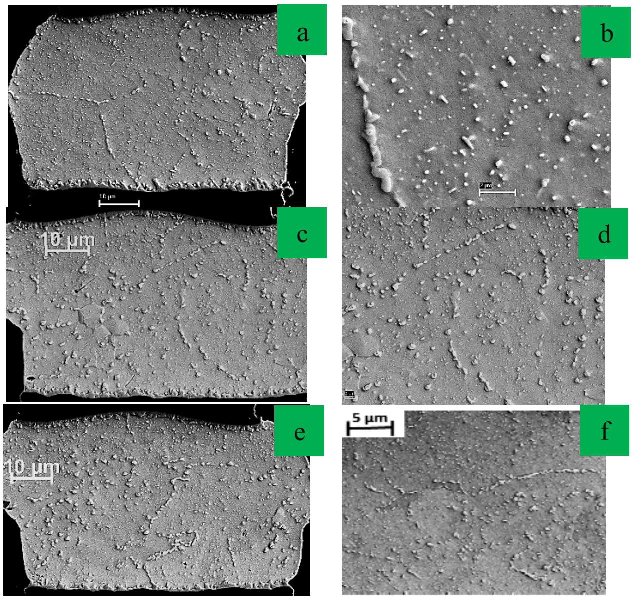

Figure 8. SEM images of multi-grain structures in 70 µm diameter Cu pillar solder joints formed with LR shown at magnifications chosen for quantitative metallography: (a), (c) and (e) 4000×, (d) and (f) 10,000×, and (b) 20,000×.

Generally, Ag_3Sn precipitates were found to be spherical in these samples produced at high cooling rates, consistent with previous observations [18-29]. The number densities of Ag_3Sn particles varied from approximately 0.6 to 0.8μm^{-2}, smaller values than observed previously for Cu pillar solder joints of similar diameters and solder compositions, but produced by MR.

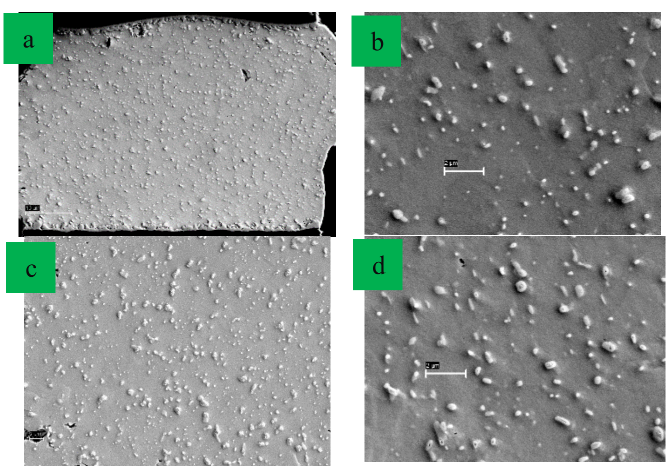

Figure 9. SEM images of interlaced grain structures in 70 µm diameter Cu pillar solder joints formed with LR shown at magnifications chosen for quantitative metallography: (a) 4000×, (c) 10,000×, and (b) and (d) 20,000×.

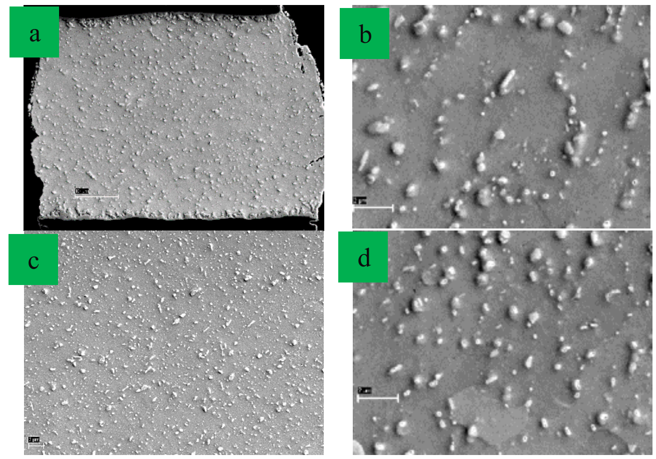

Figure 10. SEM images of single grain structures in 70 µm diameter Cu pillar solder joints formed with LR shown at magnifications chosen for quantitative metallography: (a) 4000×, (c) 10,000×, and (b) and (d) 20,000×.

Mass Reflow

Optical images with crossed polarizers, and SEM images, in Figure 11 show the microstructures of Cu pillar solder joints otherwise similar to those above, but instead produced using MR. The Sn grain morphologies, as elucidated by optical microscopy with crossed polarizers, are displayed in the left hand side of Figure 11. Once again, it was found that Sn grain morphologies could be characterized as single grained (e.g., Fig. 11(a)), multi-grained (Fig. 11(c)), or interlaced (Fig. 11(e)). The Ag_3Sn precipitate morphologies were examined for MR server solder joints using SEM, as displayed in Figs. 11 and 12. The SEM images were captured at the relatively low instrument magnification of 4000×. Figure 12 shows some select images of Ag_3Sn particles in multi-grain Sn structures taken at the various instrument magnifications used for quantitative metallography.

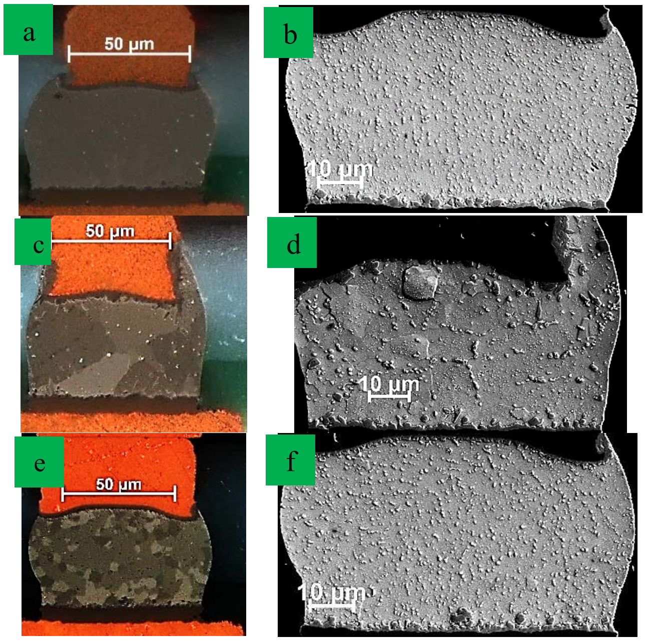

Figure 11. Cu pillar joints (server package 70µm diameter) formed with convection MR. Left side: cross-polarizer images showing the Sn grain morphology, Right side: SEM images for the same sample; (a) and (b) single grain, (c) and (d) multigrain, (e) and (f) interlaced Sn grain morphology.

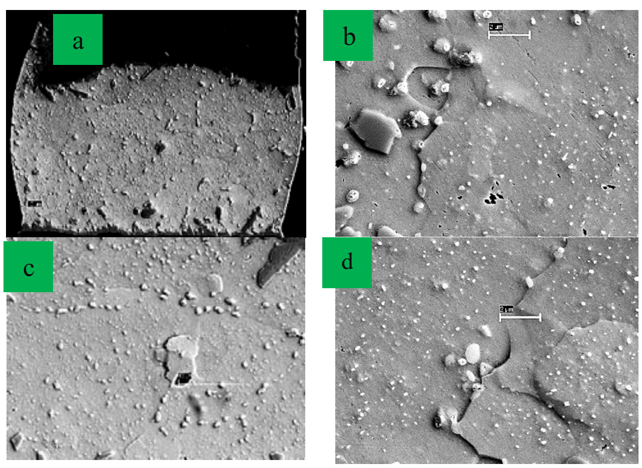

Figure 12. SEM images of 70 µm Cu pillar solder joints formed using convection MR as used for quantitative metallography. Original SEM magnifications: (a) 4000×, (c) 10,000×, and (b) and (d) 20,000×.

Generally, Ag_3Sn precipitates were found to be spherical in these samples with cooling rates close to $1^oC/s$, consistent with previous observations [12-29]. The number densities of Ag_3Sn particles varied from approximately 1.1 to $1.4\mu m^{-2}$, similar to values observed previously for Cu pillar solder joints of similar diameters and solder compositions (and produced by MR). Measured IMC thickness are listed in Table 5.

Correlation of Ag_3Sn and Sn grain morphologies

Figures 7 and 11 provide comparisons of Sn grain morphologies and Ag_3Sn morphologies for a number of different Cu pillar solder joints produced by LR and MR, respectivley. These representative micrographs reveal correlations between the Sn grain morphology and the Ag_3Sn morphology for both reflow techniques. The distribution of Ag_3Sn precipitates is more homogeneous for single grain samples than for multi grain Cu pillar solder joints or for interlaced solder joints (Figs.7 and 11). Ag_3Sn precipitates tend more to be distributed in continuous lines in multi grained and interlaced samples, lines which apparently coincide with the near 60^o grain boundaries in the multi grained and interlaced samples.

Although spatial distributions Ag_3Sn precipitates were correlated with Sn grain morphologies (Figs. 7 and 11), number densities were much more strongly correlated with reflow technique (MR or LR). The results of a quantitative comparison of the number density and size of the Ag_3Sn particles among the various Sn grain morphologies are shown in Figure 13 for both LR and MR samples. Ag_3Sn precipitate densities in MR samples tended to be more than twice that observed in LR samples, though for single grained samples this difference was much less. Furthermore, consistent with the fixed Ag_3Sn phase volume speculation, laser reflowed solder joints exhibit larger average particle sizes than the mass reflow samples. The differences in number density may reflect the reflow time differences of LR and MR, rather than cooling rate differences. The relatively short (approximately 2s) reflow times of LR may not have allowed complete dissolution of the original Ag_3Sn precipitates in the Sn melt. Upon cooling below the liquidus, any existing Ag_3Sn precipitates will begin to grow, decreasing the concentration of Ag in the remaining Sn melt. Undissolved Ag_3Sn particles in the LR cases would led to larger particles as noted in Figure 13c. When temperatures are low enough that Ag_3Sn nucleates in the undercooled Sn, forming new Ag_3Sn precipitates, lower Ag concentrations in the Sn melt would most likely lead to smaller number densities of Ag_3Sn precipitates, as observed for LR Cu pillar solder joints (particularly interlaced and multigrained LR Cu pillar solder joints). Such an explanation is consistent with the observation that Ag_3Sn precipitate number densities are closer in value in single grained samples, which in previous works were correlated with samples in which the Sn nucleated at a higher temperature [1,15,31]. In such samples the time for growth of Ag_3Sn precipitates that did not dissolve in reflow would be reduced, and the difference in number densities would be reduced, as observed. Finally, one notes that an increase in cooling rate resulted in a decrease in the Sn dendrite size, as more generally expected. This final observation is consistent with the fact that all of the Sn (much lower melting point than Ag_3Sn) dissolved during reflow, so variations of its solidification microstructure would not be expected to reflect reflow time differences of LR and MR.

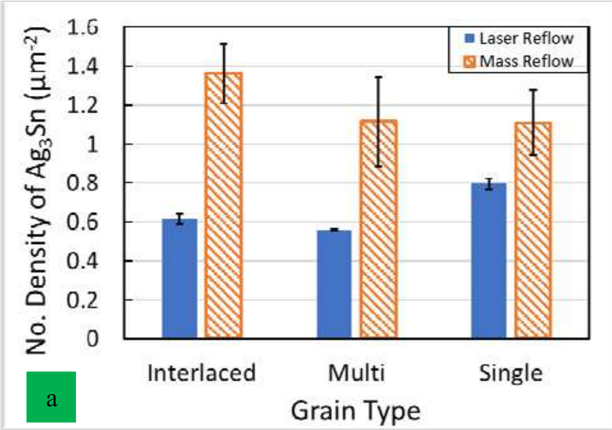

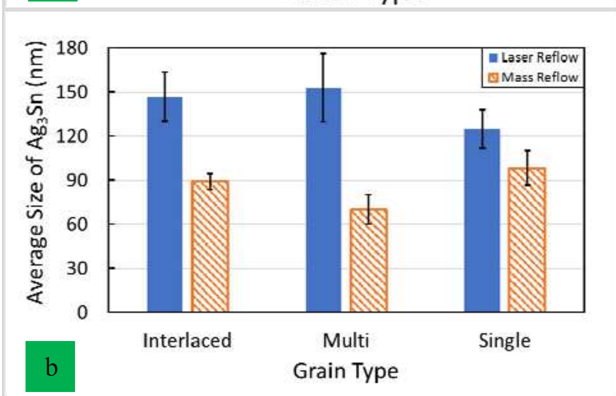

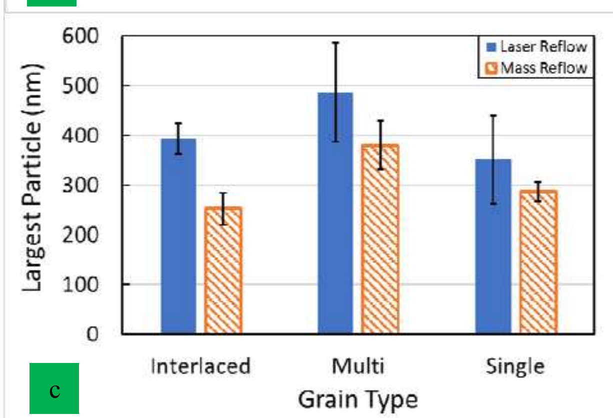

Figure 13. Quantitative measurements for MR and LR solder microstructures: (a) number density of Ag_3Sn particles, (b) average size of Ag_3Sn particles and (c) size of largest Ag_3Sn particle. Each metric is plotted by Sn grain morphology type.

Table 5. IMC's thickness for the server package

Package Type	Reflow Type	Thickness (µm)	
		IMC on Top (Ni UBM)	IMC on Bottom (Cu UBM)
Server Package	MR	1.58	1
	LR	1.1	1

Mobile Solder Joints: (23µm diameter) Ni/Sn2.5Ag/Cu

Laser Reflow

Optical images with crossed polarizers (Fig. 14), and SEM images (Fig. 15) show the microstructures of as-reflowed LR process Ni/Sn2.5Ag/Cu pillar solder joints of the mobile package. The Sn grain morphologies, as elucidated by optical microscopy with crossed polarizers, are displayed in the bottom of Fig. 14. It was found that Sn grain morphologies could be characterized as single grained or multi-grained. The Ag_3Sn precipitate morphologies were examined for LR mobile solder joints using SEM, as displayed in Fig. 15. Generally, Ag_3Sn precipitates were found to be spherical in these samples produced at high cooling rates, consistent with previous observations [12-29]. These Cu pillar solder joints (with a Cu substrate) displayed precipitate morphologies that contained numbers of relatively large, micron scale, Cu_6Sn_5 precipitates. Measured IMC thickness are listed in Table 6.

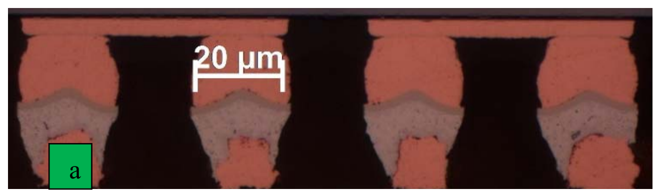

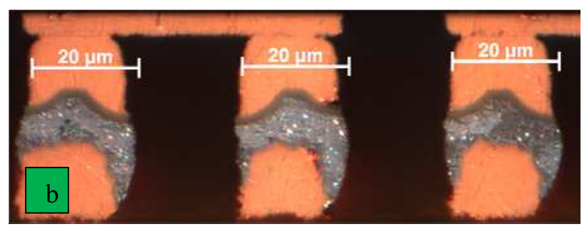

Figure 14. (a) Bright field (b) X-polarized optical micrographs showing the Cu pillars bump of the mobile chip of LR samples.

Table 6. IMC's thickness for the mobile package

Reflow Type	Thickness (µm)	
	IMC on Top (Ni UBM)	IMC on Bottom (Cu UBM)
MR	1.67	2.59
LR	1.1	1.5

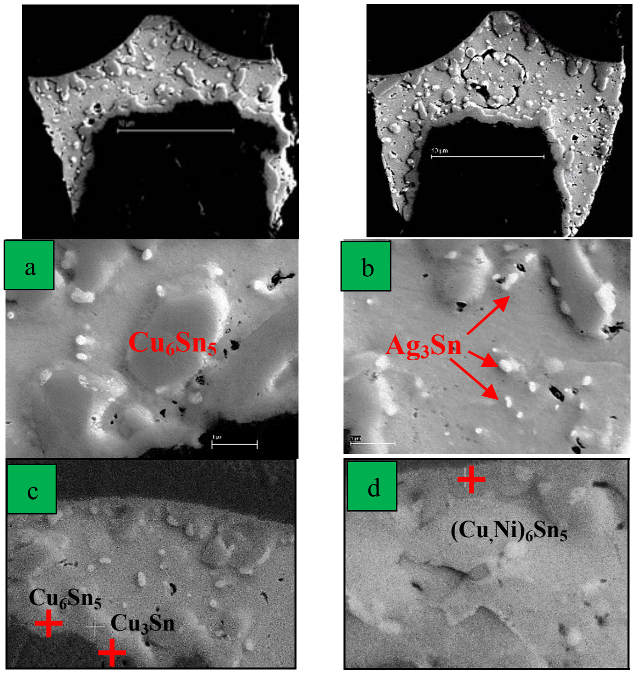

Figure 15. SEM micrograph showing the type of precipitates for the LR samples, where (a) Cu_6Sn_5 (b) Ag_3Sn precipitates, (C) Cu_6Sn_5, and Cu_3Sn, and (d) $(Cu,Ni)_6Sn_5$ IMC's

Mass Reflow

SEM images (Fig. 16) show the microstructures of as-reflowed MR process Ni/Sn2.5Ag/Cu pillar solder joints of the mobile package. The Ag_3Sn precipitate morphologies were not completely elucidated at this relatively low magnification (4000). Distinctly thicker IMC layers were observed in these MR Cu pillar solder joints (Figure 16), compared to LR samples with the same compositions (Figures 14 and 15). The MR samples had a reflow time (186s) which was much longer than that in the case of the LR mobile samples (0.8s). Measured IMC thickness are listed in Table 6.

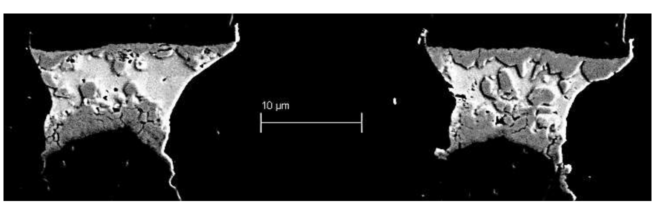

Figure 16. SEM micrograph showing the IMC at the interfaces of MR samples. It found to be thicker than the IMC of the LR samples.

CONCLUSION

While the morphology of individual Ag_3Sn particles was not sensitive to the large increases in cooling rate associated with LR, significant variations in the morphology of these Cu pillar solder joints were correlated with variations in time above the liquidus associated with LR. For cooling rates from the melt of both 1.3 and 100 $^oC/s$, Ag_3Sn precipitates were found to be spherical, with a range of submicron diameters. Relatively large, factor of two decreases in the number density of these Ag_3Sn precipitates were attributed to the short reflow times of the LR process. Time above the liquidus also affected the thickness of intermetallic compounds at the metallization interfaces, as would be expected. Careful adjustment of time above the liquidus could enhance implementation of laser reflow of Cu pillar solder joints.

ACKNOWLEDGEMENT

Authors would like to thank Dr. Francis Mutuku for valuable discussion on quantitative metallography of Ag_3Sn microstructures and Universal Instruments for funding the project.

REFERENCES

[1] F. Mutuku, B. Arfaei, E.J Cotts " The Influence of Processing on Strengthening Mechanisms in Pb-Free Solder Joints" Journal of Electronic Materials, V.46, (4), 2017, pp 2067–2079.
[2] K. Suganuma. K., 2011, "Advances in lead-free electronics soldering. Current Opinion in Solid State and Materials Science," V.5, (1), 2001, pp.55-64.
[3] H. Zhang, E. Perfecto ; V. L Calero-DdelC ; F. Pompeo, Electronic Components and Technology Conference, May 2015, pp 1695-1700.
[4] M. Genanu, B. Arfaei, E.Cotts, F. Mutuku, E. Perfecto, S. Pollard, A. Shorey. "Microstructure and Performance of Micro Cu Pillars Assemblies" Proceedings of SMTA International, Sep. 2016, Rosemont, IL, USA. pp. 75-82.
[5] M. Genanu, F. Mutuku, E. J. Cotts, B. Arfaei, Eric Perfecto, "Reliability Assessment and Microstructure Characterization of Cu Pillars Assembled on Si and Glass Substrates", IEEE 66th Electronic Components and Technology Conference, June 2016, pp. 1141.
[6] F. M. Mutuku, B. Arfaei., E. J. Cotts, "Effect of variation in the reflow profile on the microstructure of SnAgCu alloys", 64th IEEC, Electronic Components and Technology Conference. May, 2014, pp.1769.
[7] M. Genanu, F. Mutuku, E. J. Cotts, B. Arfaei, and Eric Perfecto. " Effect of Processing Variables on the Mechanical Reliability of Copper Pillar SnAg Solder JointsIEEE 67th Electronic Components and Technology Conference (ECTC). May, 2017, pp.423.
[8] S. K. Kang, D. Y. Shih, D. Leonard, D. W. Henderson, T. Gosselin, S. I. Cho, et al. Controlling Ag3Sn plate formation in near-ternary-eutectic Sn–Ag–Cu solder by minor Zn alloying. J Miner, Metals Mater Soc – JOM 2003, V.55, (6), pp. 61–5.
[9] B. Arfaei., F.M. Mutuku., K. Sweatman., N.C. Lee., E. Cotts., & R. Coyle. IEEC 64th, ECTC, 2014, pp. 655.
[10] X. Liu, M. Huang, Y. Zhao,C. Wu, L. Wang, J Alloys Compd, V.492, (1–2), 2010, pp. 433-438.
[11] J. H. L. Pang, L. Xu, X. Q. Shi, W. Zhou, S. L Ngoh, J. Electron Mater 2004;33–10:1219–25.
[12] L. Snugovsky, P. Snugovsky, D.D. Perovic, and J.W. Rutter. Experiments on the aging of Sn–Ag–Cu solder alloys. Mater. Sci. Technol. V. 48, 2013, pp. 193-198.
[13] R. S. Sidhu, N. Chawla, Mater. Charact., V.52 2004, pp. 225–230.
[14] S. L. Allen, M.R. Notis, R.R. Chromik, R.P. Vinci, "Microstructural evolution in lead-free solder alloys: Part I. Cast Sn–Ag–Cu eutectic," Journal of materials research, V.19, (5), 2004, pp.1417-1424.

[15] B. Arfaei, N. Kim, E.J Cotts, "Dependence of Sn Grain Morphology of Sn-Ag-Cu Solder on Solidification Temperature", Journal of Electronic Materials, V. 41, (2), 2012, pp. 362-374.
[16] R. Kinyanjui, L. P. Lehman, L. Zavalij & E. Cotts, J., "Effect of Sample Size on the Solidification Temperature and Microstructure of SnAgCu Near Eutectic Alloys", J. of Materials Reserch, V. 20, (11), 2005 , pp. 2914-2918.
[17] F. Guo, S. Choi, K. N. Subramanian, T. R. Bieler, et al. Evaluation of creep behavior of near-eutectic Sn–Ag solders containing small amount of alloy additions. Mater Sci Eng, V. 351A, 2003, pp.190–199.
[18] K. S. Kim, S. H. Huh, K. Suganuma, Effects of cooling speed on microstructure and tensile properties of Sn–Ag–Cu alloys, Mater. Sci. and Eng: A, 333 (1), 2002 pp.106-114.
[19] J. T. Berry, Effect of solidification conditions on mechanical behaviour of Al cast alloys. AFS Trans, V.78 1970, pp. 421-428.
[20] X. Liu, M. Huang, Y. Zhao,C. Wu, L. Wang, J. Alloys Compd., V. 492, (1–2), 2010, pp. 433-438.
[21] F. Ochoa, J. J. Williams, N. Chawla, Effects of cooling rate on the microstructure and tensile behavior of a Sn–35 wt% Ag solder. J Electron Mater, V. 32, 2003, pp. 1414–1420.
[22] J. Shen, Y. C. Liu, Y. J Han, H. X. Gao, C. Wei, Y. Q. Yang, Effects of cooling rates on microstructure and microhardness of lead-free Sn–35%Ag solders. Trans Nonferrous Met Soc China, V.16, 2006, pp.59–64.
[23] L. R. Garcia, W. R. Osorio, A. Garcia, The effect of cooling rate on the dendritic spacing and morphology of Ag3Sn intermetallic particles of a SnAg solder alloy, Materials and Design V. 32, 2011, pp. 3008–3012.
[24] L. Snugovsky, P. Snugovsky, D. D. Perovic & J. W. Rutter, "Effect of cooling rate on microstructure of Ag–Cu–Sn solder alloys", Materials Science and Technology, V. 21, (1), 2005.
[25] M. J. Song, J. J. Lin, C. F. Huang, H. Y. Chuang, Crystallization, morphology and distribution of Ag_3Sn in SnAgCu alloys and their influence on the vibration fracture properties. Mater Sci Eng.2007,466A, pp.9–17.
[26] D. W. Henderson, T. Gosselin, A. Sarkhel, Ag3Sn plate formation in the solidification of near ternary eutectic Sn–Ag–Cu alloys. J Mater Res, 2002, 17(11).
[27] M. Sona, K.N. Prabhu, Effect of Reflow Time on Wetting Behavior, Microstructure Evolution, and Joint Strength of Sn-2.5Ag-0.5Cu Solder on Bare and Nickel-Coated Copper Substrates. Journal of Electronic Materials, V. 45, No. 7, 2016.
[28] H. T. Lee, K. C. Huang, Effects of Cooling Rate on the Microstructure and Morphology of Sn-3.0Ag-0.5Cu Solder , Journal of Electronic Materials,V.45, (1). 2016.
[29] W. Yang, L.E. Felton, and R.W. Messler, The Effect of Soldering Process Variables on the Microstructure and Mechanical Properties of Eutectic Sn-Ag/Cu Solder JointsJ. Electron. Mater. V.24, 1995, pp.1465.
[30] J. Wilcox, M. Genanu, K. S. Kim, "Laser Reflow Flip Chip Characterization", Universal Instruments Corporation APL Conducts AREA Consortium Meeting, March 2017.
[31] D. R. Frear, Mechanics of Solder Alloy Interconnects (New York: Van Nostrand Reinhold, 1994).